

Spin-Orbit Coupling Induced Back-action Cooling in Cavity-Optomechanics with a Bose-Einstein Condensate

Kashif Ammar Yasir,^{1,2,*} Lin Zhuang,^{3,†} and Wu-Ming Liu^{1,2,‡}

¹*Beijing National Laboratory for Condensed Matter Physics,*

Institute of Physics, Chinese Academy of Sciences, Beijing 100190, China.

²*School of Physical Sciences, University of Chinese Academy of Sciences, Beijing 100190, China.*

³*School of Physics, Sun Yat-Sen University, Guangzhou 510275, P. R. China.*

We report a spin-orbit coupling induced back-action cooling in an optomechanical system, composed of a spin-orbit coupled Bose-Einstein condensate trapped in an optical cavity with one movable end mirror, by suppressing heating effects of quantum noises. The collective density excitations of the spin-orbit coupling mediated hyperfine states – serving as atomic oscillators equally coupled to the cavity field – trigger strongly driven atomic back-action. We find that the back-action not only revamps low-temperature dynamics of its own but also provides an opportunity to cool the mechanical mirror to its quantum mechanical ground state. Further, we demonstrate that the strength of spin-orbit coupling also superintends dynamic structure factor and squeezes nonlinear quantum noises, like thermo-mechanical and photon shot noise, which enhances optomechanical features of hybrid cavity beyond the previous investigations. Our findings are testable in a realistic setup and enhance the functionality of cavity-optomechanics with spin-orbit coupled hyperfine states in the field of quantum optics and quantum computation.

PACS numbers: 42.50.Wk, 37.10.De, 71.70.Ej

I. INTRODUCTION

Cavity-optomechanics provides splendid foundations in utilizing mechanical effects of light to couple optical degree of freedom with mechanical degree of freedom [1–3]. A pivotal paradigm was to cool vibrational modes of mechanical degree of freedom to its quantum mechanical ground state which has been attempted to achieve via laser radiations, electronic feedback and dynamical back-action [4–12]. The dynamical back-action is the cavity delay induced by the interactions of intra-cavity radiation pressure and the Brownian motion of the mirror which leads to cool mirror depending upon detuning [13–16]. The demonstration of cavity-optomechanics with other physical objects, like cold atomic gases [17] and Bose-Einstein condensate (BEC) [18–20], opens up various new aspects to further cool vibrational modes through atomic back-action [21–25]. However, thermo-mechanical heating, due to the quantum noises [26–30], is a major obstacle in achieving an oscillator with long phonon lifetime in quantum ground state which we intend to solve by the inclusion of spin-orbit (SO)-coupled BEC.

The SO-coupling, a stunning phenomenon describing interaction between spin of quantum particle and its momentum, has made remarkable progress in the last few years [31–33] and is essential to analyze spin-Hall effect [34, 35], topological insulators [36–39] and spintronic devices [40]. The demonstration of SO-coupling in one-dimensional optical lattices [41–52] and optical cavities

[53–55] enables us to utilize this phenomenon in optomechanical environment. The SO-coupling induces significant variations in cavity radiation pressure by separating atomic mode in hyperfine spin-states which gives rise to self-confinement via dynamical back-action [1, 56–58]. Further, dynamic structure factor, a phenomenon describing density fluctuations and mean energy of excited quasi-particles, is crucially important in quantum many-body systems [59] and provides explanation of quasi-particle evolution under noise effects [60–62].

In this paper, we report the SO-coupling induced back-action cooling mechanism in a hybrid optomechanical cavity with SO-coupled BEC and one moving end mirror in the presence of quantum noises. We show that the SO-coupling induced features modify intra-cavity atomic back-action which not only leads to maneuver low-temperature dynamics of atomic mode but also helps

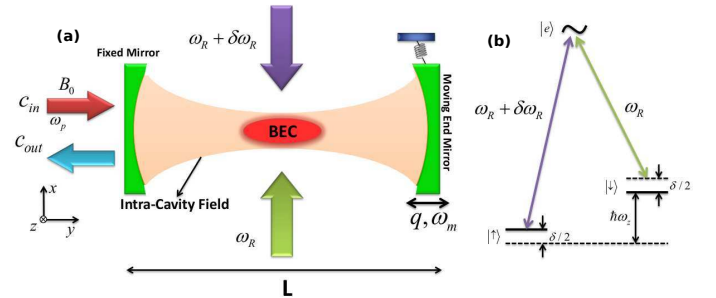


FIG. 1. (Color online) (a) Schematic diagram of spin-orbit (SO)-coupled ^{87}Rb Bose-Einstein condensate (BEC) trapped inside a high- Q Fabry-Pérot cavity with one moving end mirror, where \hat{y} -axis is the cavity axis and \hat{x} -axis is the direction of incident Raman beams. (b) Energy level configuration of SO-coupled BEC.

* kayasir@iphy.ac.cn

† stszhl@mail.sysu.edu.cn

‡ wliu@iphy.ac.cn

in ground state cooling of vibrational modes of the cavity mirror. Further, the coupling of mechanical mirror with cavity modifies the eigenenergy spectrum of hyperfine states via transformation of phonons to atomic degree of freedom and provides a way to tune quantum phase transitions in BEC. Furthermore, we compute dynamic structure factor by manipulating two frequency auto-correlation of photons leaking-out from cavity and observe the influence of SO-coupling on dynamic structure factor.

II. CAVITY-OPTOMECHANICS WITH SO-COUPLED BEC

The system consists of a high- Q Fabry-Pérot cavity, with one fixed and one movable mirror, containing SO-coupled BEC illuminated along \hat{y} -axis and coherently driven by single-mode optical field with frequency $\omega_p = \omega_R + \delta\omega_R = 8.8 \times 2\pi$ MHz, see Fig. 1(a). To produce SO-coupling, we chose two internal atomic pseudo-spin-states in $N = 1.8 \times 10^5$ ^{87}Rb bosonic particles having $F = 1$ electronic ground manifold of $5S_{1/2}$ electronic levels labeled as $|\uparrow\rangle = |F = 1, m_F = 0\rangle$ (pseudo-spin-up) and $|\downarrow\rangle = |F = 1, m_F = -1\rangle$ (pseudo-spin-down), as shown in Fig. 1(b). The magnetic $10G$ bias field B_0 is applied along cavity axis (\hat{y} -axis) to induce Zeeman shift $\hbar\omega_z$, where $\omega_z \approx 4.8 \times 2\pi$ kHz. Two counter-propagating Raman lasers along \hat{x} -axis, with wavelength $\lambda = 804.1nm$ and detuning $\delta = 1.6E_R$, interact with atomic spin-states in opposite direction. The frequencies of these Raman beams are ω_R and $\omega_R + \delta\omega_R$, respectively, with constant frequency difference $\delta\omega_R = \omega_z + \delta/\hbar \simeq 4.8 \times 2\pi$ MHz. $\mathbf{k}_L = \hbar\mathbf{k}_y = \sqrt{2\pi\hbar}/\lambda$ and $E_R = (\hbar\mathbf{k}_y)^2/2m_a = 20 \times 2\pi$ kHz represent unit-less momentum and energy, respectively. The mechanical mirror is coupled to the cavity mode, oscillating with frequency $\omega_c = 4 \times 2\pi$ MHz and detuning $\Delta_c = \omega_p - \omega_c = \delta\omega_R$, via radiation pressure force [1, 18].

The system Hamiltonian consists of three parts, $\hat{H} = \hat{H}_a + \hat{H}_m + \hat{H}_f$. In strong detuning regime and under rotating-wave approximation, the many-body Hamiltonian for atomic mode (H_a) is given as [42, 53, 54],

$$\hat{H}_a = \int d\mathbf{r} \hat{\psi}^\dagger(\mathbf{r}) \left(H_0 + V_{LAT} \right) \hat{\psi}(\mathbf{r}) + \frac{1}{2} \int d\mathbf{r} \sum_{\sigma, \sigma'} U_{\sigma, \sigma'} \hat{\psi}_\sigma^\dagger(\mathbf{r}) \hat{\psi}_{\sigma'}^\dagger(\mathbf{r}) \hat{\psi}_{\sigma'}(\mathbf{r}) \hat{\psi}_\sigma(\mathbf{r}), \quad (1)$$

where m_a is the mass of an atom, $\hat{\psi} = [\hat{\psi}_\uparrow, \hat{\psi}_\downarrow]^T$ represents bosonic field operator for pseudo-spin-up and -down atomic states. $H_0 = \hbar^2 \mathbf{k}^2 \sigma_0 / 2m_a + \tilde{\alpha} \mathbf{k}_x \sigma_y + \frac{\delta}{2} \sigma_y + \frac{\Omega_z}{2} \sigma_z$ describes single-particle Hamiltonian containing SO-coupling terms [33, 63], where $\tilde{\alpha} = E_R / \mathbf{k}_L$ is the strength of SO-coupling. $\delta = -g\mu_B B_z$ and $\Omega_z = -g\mu_B B_y$ are related to the Zeeman field effects along \hat{z} and \hat{y} axis, respectively. $\sigma_{x,y,z}$ represents 2×2 Pauli matrices under pseudo-spin rotation and σ_0 is a unit matrix

[42, 63]. $V_{LAT} = \hbar \hat{c}^\dagger \hat{c} U_0 [\cos^2(kx) + \cos^2(ky)]$ is the intra-cavity optical lattice under assumption $k_x = k_y = k$ and both atomic states are equally coupled to the cavity because of having same motional quantum state [54, 64]. $\hbar \hat{c}^\dagger \hat{c} U_0$ is optical potential depth with atom-photon coupling $U_0 = g_0^2 / \Delta_a$, where g_0 is the vacuum Rabi frequency and Δ_a is far-off detuning between field frequency and atomic transition frequency ω_0 . Here, $\hat{c}(\hat{c}^\dagger)$ are annihilation (creation) operators for cavity mode. Finally, last term explains many-body intra-species and inter-species interactions for atomic spin-states, where $\sigma, \sigma' \in \{\uparrow, \downarrow\}$. $U_{\sigma, \sigma'} = 4\pi a_{\sigma, \sigma'}^2 \hbar^2 / m_a$ accounts for strength of atom-atom interactions, where $a_{\sigma, \sigma'}$ is the s-wave scattering length.

The Hamiltonian for moving end mirror is $\hat{H}_m = \hbar\omega_m \hat{b}^\dagger \hat{b} - i\hbar \frac{g_m}{\sqrt{2}} \hat{c}^\dagger \hat{c} (\hat{b}^\dagger + \hat{b})$, where first term describes the motion of mechanical mirror with frequency ω_m and $\hat{b}(\hat{b}^\dagger)$ are annihilation (creation) operators for mechanical mirror with commutation relation $[\hat{b}^\dagger, \hat{b}] = 1$. Second term accommodates mechanical mirror coupling with cavity mode with coupling strength $g_m = \sqrt{2}(\omega_c/L)x_0$, where $x_0 = \sqrt{\hbar/2m\omega_m}$ is zero point motion of mechanical mirror having mass m . $\hat{H}_c = \hbar\Delta_c \hat{c}^\dagger \hat{c} - i\hbar\eta(\hat{c} - \hat{c}^\dagger)$, where first term is the strength of cavity mode and second part is associated with its coupling with external pump field with strength $|\eta| = \sqrt{P\kappa/\hbar\omega_p}$, where P is the input field power.

We substitute plane-wave ansatz $\hat{\psi}(\mathbf{r}) = e^{i\mathbf{k}\cdot\mathbf{r}} \hat{\phi}$, where $\hat{\phi} = [\hat{\phi}_\uparrow, \hat{\phi}_\downarrow]^T$, in atomic mode Hamiltonian H_a by considering homogeneous atomic modes distribution with normalization condition $|\hat{\phi}_\uparrow|^2 + |\hat{\phi}_\downarrow|^2 = N$. We assume that the strengths of intra-species interactions of both spin-states are equal with each other and are defined as, $U_{\uparrow, \uparrow} = U_{\downarrow, \downarrow} = U$. Similarly, inter-species interactions can be modeled as, $U_{\uparrow, \downarrow} = U_{\downarrow, \uparrow} = \varepsilon U$, where parameter ε depends upon the incident laser configuration [33]. Under these considerations, we solve equation H_a and compute quantum Langevin equations for the system by using standard quantum-noise operators to include quantum noises and dissipations associated with the system [21, 50]. The quantum Langevin equation helps us in developing coupled and time dependent set of equations, containing noise operators for optical, mechanical and atomic degrees of freedom,

$$\frac{d\hat{c}}{dt} = \dot{\hat{c}} = (i\tilde{\Delta} + i\frac{g_m}{\sqrt{2}}(\hat{b} + \hat{b}^\dagger) - ig_a \hat{\phi}^\dagger \hat{\phi} - \kappa) \hat{c} + \eta + \sqrt{2\kappa} a_{in}, \quad (2)$$

$$\frac{d\hat{b}}{dt} = \dot{\hat{b}} = -\omega_m \hat{b} - \frac{g_m}{\sqrt{2}} \hat{c}^\dagger \hat{c} - \gamma_m \hat{b} + \sqrt{\gamma_m} f_m, \quad (3)$$

$$\frac{d\hat{\phi}}{dt} = \dot{\hat{\phi}} = \left(\frac{\hbar\mathbf{k}^2 \sigma_0}{2m} + \tilde{\alpha} \mathbf{k}_x \sigma_y + \frac{\delta}{2} \sigma_y + \frac{\Omega_z}{2} \sigma_z - \gamma_a + g_a \hat{c}^\dagger \hat{c} \right) \hat{\phi} + \frac{1}{2} U \hat{\phi}^\dagger \hat{\phi} \hat{\phi} + \frac{1}{2} \varepsilon U \hat{\phi}_\sigma^\dagger \hat{\phi}_{\sigma'} \hat{\phi}_{\sigma'} + \sqrt{\gamma_a} f_a, \quad (4)$$

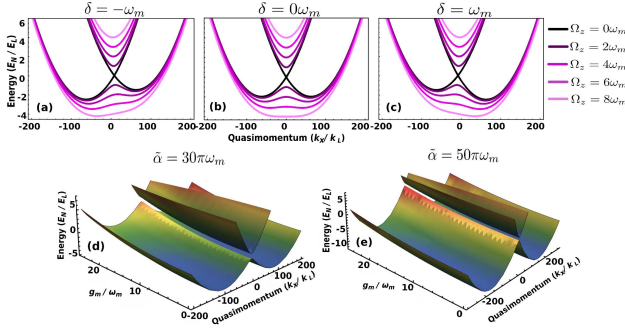


FIG. 2. (Color online) (a-c) Eigenenergies spectrum E_N of spin-orbit (SO)-coupled Bose-Einstein condensate (BEC) as a function of quasi-momentum $\mathbf{k}_x/\mathbf{k}_L$ for different Ω_z/ω_m and δ/ω_m , when $g_m/\omega_m = 0.1$ and $\alpha/\omega_m = 20\pi$. (It should be noted that we consider $\mathbf{k}_y = \mathbf{k}_z = 0$ because SO-coupling is occurring only in the direction of \hat{x} -axis.) The black curve represents dispersion at $\Omega_z/\omega_m = 0$ while magenta shaded curves (from darkest to lightest) correspond to $\Omega_z/\omega_m = 2, 4, 6, 8$, respectively. (a), (b) and (c) show the behavior of dispersion E_N for $\delta/\omega_m = -1, 0, 1$, respectively. (d) and (e) show dispersion E_N versus $\mathbf{k}_x/\mathbf{k}_L$ and g_m/ω_m , with $\alpha/\omega_m = 30\pi$ and $\alpha/\omega_m = 50\pi$, respectively, at $\Omega_z = \omega_m$ and $\delta/\omega_m = 0$. The other parameters used are $U/\omega_m = 5.5$, $\varepsilon/\omega_m = 0.1$, $\kappa/\omega_m = 0.1$, $\gamma_a/\omega_m = 0.01$, $\gamma_m/\omega_m = 0.05$ and mechanical mirror frequency $\omega_m \approx \omega_c - \omega_p$.

where $\tilde{\Delta} = \Delta_c - NU_0/2$ is the modified detuning of the system and \hat{c}_{in} is Markovian input noise operator associated with intra-cavity field, having zero-average $\langle \hat{c}_{in}(t) \rangle = 0$ and delta-correlation $\langle \hat{c}_{in}(t) \hat{c}_{in}^\dagger(t') \rangle = \delta(t-t')$ under the condition $\hbar\omega_c \gg k_B T$. The term γ_m describes mechanical energy decay rate of the moving end mirror and \hat{f}_m is noise operator (or zero-mean Langevin-force operator) connected with the Brownian motion of mechanical mirror and can be defined by using non-Markovian correlation [21, 50] $\langle \hat{f}_m(t) \hat{f}_m^\dagger(t') \rangle = \frac{\gamma_m}{2\pi\omega_m} \int d\omega e^{-i\omega(t-t')} [1 + \text{Coth}(\frac{\hbar\omega}{2k_B T})]$. The external harmonic trapping potential of the condensate, which we have ignored so far because it appeared to be spin independent, cause the damping of the atomic motion. The parameter γ_a represents such damping of atomic dressed states motion while \hat{f}_a is the associated noise operators assumed to be Markovian with delta-correlation $\langle \hat{f}_a(t) \hat{f}_a^\dagger(t') \rangle = \delta(t-t')$ under the condition $\hbar\Omega \gg k_B T$. Further, $\sigma, \sigma' \in \{\uparrow, \downarrow\}$ and $g_a = \frac{\omega_c}{L} \sqrt{\hbar/m_{bec} 4\omega_r}$ is the coupling of atomic mode with intra-cavity field, having effective BEC frequency $\Omega = 4\omega_r$ and mass $m_{bec} = \hbar\omega_c^2/(L^2 U_0^2 \omega_r)$, where $\omega_r = 3.8 \times 2\pi \text{kHz}$ is the recoil frequency of atoms and $L = 1.25 \times 10^{-4} \text{m}$ is the cavity length.

III. CONDENSATE DISPERSION SPECTRUM

The eigenenergy spectrum is calculated from time-dependent quantum Langevin equations (for details see

Appendix A). The SO-coupling will create two minima corresponding to lowest energy-levels of atomic spin-states, as illustrated in Fig. 2. At $\Omega_z/\omega_m = 0$, no band-gap appears between lower and upper dispersion states causing the phase mixing of atomic dressed states. However, in presence of Raman coupling, the band-gap between upper $E_N > 0$ and lower $E_N < 0$ dispersion states appears in the form of Dirac-cone which increases with the increase in Raman coupling. The higher values of Ω_z/ω_m merge two minima corresponding to the dressed states into single minima causing quantum phase transitions from mixed phase to separate phase of atomic mode. It can also be seen that the non-zero Raman detuning $\delta/\omega_m \neq 0$ leads to the symmetry-breaking of dispersion over quasi-momentum. For the small value of Raman coupling ($\Omega_z < 4\omega_m$), the dispersion appears in the form of double-well potential in the quasi-momentum which leads to the zero group velocity of atoms [65]. The asymmetric behavior indicates rapid population transfer and enhancement in band-gap induced features of hyperfine states in cavity environment. Moreover, it is noted that because of cavity confinement, the atomic quasi-momentum $\mathbf{k}_x/\mathbf{k}_L$ interacts with the optical mode along cavity axes. Thus, SO-coupled BEC face an anisotropic potential which leads towards spatial spread of BEC energy spectrum along cavity axis, as can be seen in Fig. 2

The coupling between atomic states and intra-cavity potential is disturbed by the existence of mechanical mirror, and vice-versa, when the atomic modes become resonant with the optical sideband. At this point, atomic spin states will absorb some phonons emitted by the mechanical mirror via cavity mode and will behave as a phononic-well. Therefore, the increase in mirror-field coupling gives rise to atomic-state energy levels, as shown in Fig. 2(d) and 2(e), which provides precise control over the dispersion relation of atomic energy spectrum and quantum phase transitions of BEC.

IV. ATOMIC DENSITY-NOISE SPECTRUM

We calculate density-noise spectrum (DNS) of atomic spin states by taking two-frequency auto-correlation of the frequency domain solution of quantum Langevin equations, $S_{\uparrow,\downarrow}(\omega, \Delta) = \frac{1}{4\pi} \int e^{-i(\omega+\omega')t} \langle \delta\hat{q}_{\uparrow,\downarrow}(\omega) \delta\hat{q}_{\uparrow,\downarrow}(\omega') + \delta\hat{q}_{\uparrow,\downarrow}(\omega') \delta\hat{q}_{\uparrow,\downarrow}(\omega) \rangle d\omega'$, where $\delta\hat{q}_{\uparrow,\downarrow}$ are dimensionless position quadratures of spin states defined as, $\delta\hat{q}_{\uparrow,\downarrow} = \frac{1}{\sqrt{2}}(\hat{\varphi}_{\uparrow,\downarrow} + \hat{\varphi}_{\uparrow,\downarrow}^\dagger)$. Here the effective system detuning is $\Delta = \tilde{\Delta} - g_m q_s + g_a N$, where q_s is steady-state position quadratures of mechanical mirror, while $G_m = \sqrt{2}g_m|c_s|$ and $G_a = \sqrt{2}g_a|c_s|$ are the effective couplings of intra-cavity field with mechanical mirror and atomic modes, respectively, tuned by the steady-state cavity mode amplitude $c_s = \frac{\eta}{\kappa + i\Delta}$ (for detailed calculations see Appendix B and C). By considering the correlation operators of Markovian and Brownian noises in frequency domain [21, 22, 66, 67], we

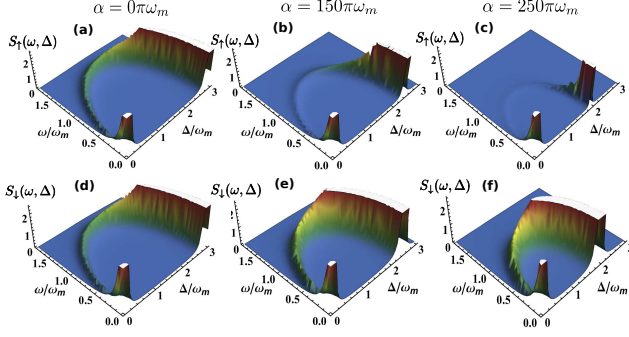


FIG. 3. (Color online) (a-c) Illustrate DNS $S_{\uparrow}(\omega, \Delta)$ as a function of Δ/ω_m and ω/ω_m for $\alpha/\omega_m = 0\pi, 150\pi$ and 250π , respectively, when $\Omega_z = \omega_m$, $\delta/\omega_m = 1$ and $G_a/\omega_m = 28.5$. (Note: The color configuration corresponds to the strength of DNS.) Similarly, (d-f) demonstrate DNS $S_{\downarrow}(\omega, \Delta)$ for $\alpha/\omega_m = 0\pi, 150\pi$ and 250π , respectively. Here $G_m/\omega_m = 1.5$, $\Omega/\omega_m = 70.8$, $\omega_m = 3.8 \times 2\pi\text{kHz}$ and the thermal reservoir temperature is taken as $T = 300\text{K}$.

plot the DNS for pseudo spin- \uparrow and spin- \downarrow atomic states as shown in Fig. 3.

The inclusion of SO-coupling in trapped-atoms modifies atomic back-action generated by the interaction of intra-cavity radiation pressure with BEC. These modifications enhance the cavity induced self-regulatory mechanism of atomic mode. In the absence of SO-coupling ($\alpha/\omega_m = 0\pi$), both $S_{\uparrow}(\omega, \Delta)$ and $S_{\downarrow}(\omega, \Delta)$ behave in a similar way as shown in Fig. 3(a) and 3(d) [21, 22], where $\alpha = \tilde{a}k_x$ is the effective strength of SO-coupling. Both the cooling as well as heating mechanisms are observable because area under $S_{\uparrow}(\omega, \Delta)$ describes the effective temperature of atomic mode, as shown in effective temperature calculation of mechanical mirror in next section. One can observe a semi-circular structure appearing with the increase in Δ/ω_m caused by the red-shift in the peak frequency of $S_{\uparrow}(\omega, \Delta)$. Height of the structure initially decreases with increase in Δ/ω_m towards ω/ω_m but shortly again starts rising along the semi-circular structure. The optimal cooling is achieved at $\Delta = \omega_m/2$ with a considerable shrink in the area underneath atomic DNS.

In the presence of α/ω_m , $S_{\uparrow}(\omega, \Delta)$ and $S_{\downarrow}(\omega, \Delta)$ start behaving in a different manner because of the emergence of Zeeman shift among the hyperfine atomic states with SO-coupling. For $S_{\uparrow}(\omega, \Delta)$, the height of semi-circular structure is suppressed due to the energy transformation via intra-cavity potential, as can be seen in Fig. 3(b) and 3(c), where $\alpha/\omega_m = 150\pi$ and 250π , respectively. The optimal cooling point is now shifted to $\Delta/\omega_m = 1$. The existence of SO-coupling not only decreases the area underneath $S_{\uparrow}(\omega, \Delta)$ but also suppresses the radius of that semi-circular structure providing controlled cooling of atomic mode. However, at $\alpha/\omega_m \neq 0\pi$, $S_{\downarrow}(\omega, \Delta)$ behave differently because of more interaction with quantum noise effects, as shown in Fig. 3(e) and 3(f). Now the height of semi-circular structure appearing in $S_{\downarrow}(\omega, \Delta)$ is

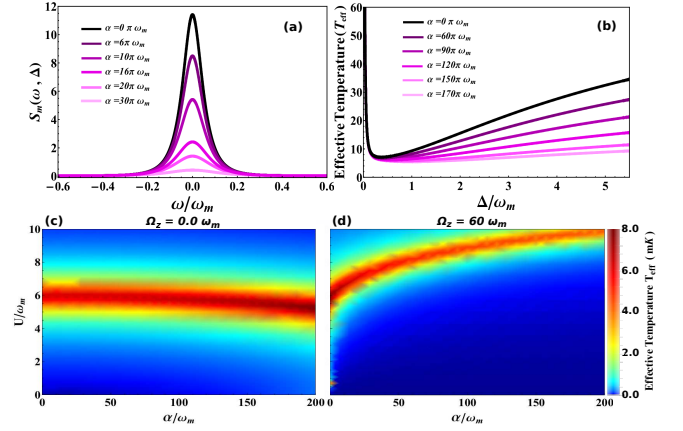


FIG. 4. (Color online) (a) Illustrates $S_m(\omega, \Delta)$ versus normalized frequency ω/ω_m at $\Delta/\omega_m = 1.8$, $G_m/\omega_m = 10$ and $G_a/\omega_m = 20$. The black curve is for $\alpha/\omega_m = 0\pi$ and magenta curves from dark shade to light shade represent $\alpha/\omega_m = 6\pi, 10\pi, 16\pi, 20\pi$ and 30π , respectively. (b) Describes T_{eff} (in units of mK) versus Δ/ω_m at $\omega/\omega_m = 0.1$, $G_m/\omega_m = 10$ and $G_a/\omega_m = 5$. Similarly, the black corresponds to $\alpha/\omega_m = 0\pi$ while shaded curves from darkest to lightest represent $\alpha/\omega_m = 60\pi, 90\pi, 120\pi, 150\pi$ and 170π , respectively. (c) and (d) show T_{eff} , as a function of α/ω_m and U/ω_m , at $\Omega_z/\omega_m = 0$ and 80 , respectively. Here, $G_m/\omega_m = 18$, $G_a/\omega_m = 16$ and $\alpha/\omega_m = 30\pi$.

being increased with increase in SO-coupling. The SO-coupling induced Zeeman field effect generates the energy gap between dressed states by increasing and decreasing the ground state energies of pseudo spin- \downarrow and pseudo spin- \uparrow states, respectively. Therefore, by increasing SO-coupling, spin- \downarrow state will interact with more noise effects and get heated because of having more ground state energy as compared to spin- \uparrow state. However, it can be controlled by varying system parameters and the radius of semi-circular structure still appears to be decreasing with SO-coupling due to cavity mediated self-confinement via back-action. Further, in presence of SO-coupling, atom-atom interactions will effect similarly the low-temperature dynamics of atomic mode, as explained in Appendix E.

V. MECHANICAL MIRROR COOLING

The effective temperature of mechanical mode (T_{eff}) is calculated by formula $T_{eff} = \langle E_m \rangle / k_B$, where $\langle E_m \rangle = m\omega_m^2 \langle \delta \hat{q}^2 \rangle / 2 + \langle \delta \hat{p}^2 \rangle / 2m = m\omega_m^2 (n_{eff} + 1/2)$, corresponds to the mean energy which is experimentally measured by calculating area underneath DNS of mechanical mirror $S_m(\omega, \Delta) = \frac{1}{4\pi} \int e^{-i(\omega+\omega')t} \langle \delta \hat{q}(\omega) \delta \hat{q}(\omega') + \delta \hat{q}(\omega') \delta \hat{q}(\omega) \rangle d\omega'$, where $\delta \hat{q}$ is dimensionless position quadrature of mechanical mirror defined as, $\delta \hat{q} = \frac{1}{\sqrt{2}}(\hat{b} + \hat{b}^\dagger)$ (for detail see Appendix B and C). n_{eff} is the effective phonon number which should be less than one in order to achieve ground state cooling. The position

and momentum variances are related to DNS, $\langle \delta \hat{\mathcal{R}}^2 \rangle = \frac{1}{2\pi} \int S_{\mathcal{R}}(\omega, \Delta) d\omega$, where \mathcal{R} is a generic operator representing position $\delta \hat{q}$ and momentum $\delta \hat{p}$ quadrature of mechanical mirror. Here the DNS of mechanical mirror in momentum space is defined as $S_{m(p)}(\omega, \Delta) = m^2 \omega_m^2 S_m(\omega, \Delta)$, where m is the effective mass of mechanical mirror.

The cooling mechanism for mechanical mirror, which can simply be explained by thermodynamic arguments, only occurs when the intra-cavity optical sideband is centered at ω_m which is in fact a resolved-sideband regime. Therefore, the BEC should also oscillate at optical sideband frequency in order to absorb excitation energies of the mirror from cavity mode otherwise mirror temperature will be unaffected. The implication of SO-coupling splits atomic mode into dressed spin states – acting like two atomic mirrors equally coupled to the cavity – which will modify atomic back-action inside the cavity. This phenomenon enables us to transfer more excitation energies in the form of phonons from mechanical mirror to atomic degree of freedom. Fig.4(a) illustrates such effects where the suppression of mechanical mirror DNS $S_m(\omega, \Delta)$ can be seen with the increase in SO-coupling. The SO-coupling suppresses the heating effects induced by the Brownian motion of the mirror and enhances back-action cooling of oscillating mirror. Fig.4(a) demonstrates mirror DNS at system detuning $\Delta/\omega_m = 1.8$. If we change system detuning, it will modify mirror DNS by increasing or decreasing its strength but the effects of SO-coupling on mirror DNS will remain the same, as discussed in Appendix F. Further, the SO-coupling reduces T_{eff} over a wide range of detuning because of energy transformation via modified back-action, as shown in Fig.4(b), where optimal temperature is decreasing with the increase in SO-coupling. This implies, like atomic-field coupling and atom-atom interactions (as discussed in Appendix G) [13–16, 23–25], SO-coupling significantly alters ground state properties of mechanical mirror. Thus, SO-coupling provides another handle to achieve and sustain ground state cooling which is even beyond the previous back-action cooling mechanism.

To further analyze the influence of SO-coupled dressed states on mechanical mirror, we plot T_{eff} , as a function of U/ω_m and α/ω_m , in absence (Fig.4(c)) and in presence (Fig.4(d)) of Raman coupling Ω_z/ω_m . At $\Omega_z/\omega_m = 0$, the maximum value of T_{eff} appears to be approximately centered at $U/\omega_m \approx 6$ and remains saturated with increase in α/ω_m . One can state that the maximum value of T_{eff} shows a kind of localized behavior with SO-coupling which is similar to the results presented in reference [23]. On the other hand, in presence of Raman coupling, T_{eff} shows squeezed and exponential behavior with α/ω_m , as illustrated in Fig.4(d). The SO-coupling in presence of strong Raman coupling, which transforms atomic dispersion spectrum into single minima, absorbs more mirror excitation energies and manipulates atom-atom interactions effects on mirror temperature by modifying back-action. Intuitively saying, the higher values of

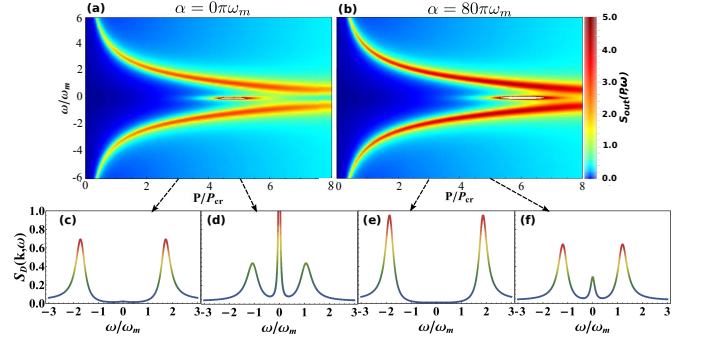


FIG. 5. (Color online) (a) and (b) DNS of optical field leaking-out of cavity $S_{out}(P, \omega)$ (in units of W/Hz), versus P/P_{cr} and ω/ω_m , for $\alpha/\omega_m = 0\pi$ and 80π , respectively. (c-f) show dynamic structure factor (in units of $1/Hz$) corresponding to the out-going optical mode DNS versus ω/ω_m for different values of P/P_{cr} . SO-coupling $\alpha/\omega_m = 0\pi$ (80π) for (c) and (d). While the strength of SO-coupling is $\alpha/\omega_m = 80\pi$ for (e) and (f). Here $G_m/\omega_m = 1.5$, $G_a/\omega_m = 0.9$, $U/\omega_m = 5.5$ and $\delta/\omega_m = 0$.

Raman coupling change quantum phase of trapped atoms causing the alteration in their many-body interactions as well as in SO-coupling effects. Therefore, the suppressed and nonlinear behavior of T_{eff} is caused by the emergence of band-gap induced quantum phase transitions of BEC and can be further enhanced by increasing Ω_z/ω_m providing control over temperature of mechanical mirror [13, 14, 23].

VI. DYNAMIC STRUCTURE FACTOR

We analyze dynamic structure factor by computing Fourier domain auto-correlations of light leaking-out of the cavity. The resultant dynamic structure factor is given as [62], $S_D(k, \omega) = \frac{4(\kappa^2 + \Delta^2)}{N\eta^2} (\frac{1}{2\pi} S_{out}(P, \omega) + n_s^2 \delta(\omega))$, where n_s is the steady-state photon number and $S_{out}(P, \omega)$ is DNS of out-going optical mode (see Appendix D). The frequency ω is referred to the shifted frequency of input field after interacting with the system which causes inelastic photon scattering.

In absence of SO-coupling, $S_{out}(P, \omega)$ contains two sidebands at $\omega < 0\omega_m$ and $\omega > 0\omega_m$ caused by the incoherent creation and annihilation of quasi-particles [62], respectively, see Fig.5(a). If we increase the input power, both the sidebands tend to move towards $\omega = 0\omega_m$ because of quantum fluctuations which decrease the spectral densities of quasi-particles. Intuitively, it is referred to the scattering of intra-cavity optical mode at Bragg planes in the density-modulated cloud [68, 69]. Both the sidebands seem to get mixed with each other due to the presence of another secondary structure approximately at $P \approx 6P_{cr}$. The secondary structure, which is centered at $\omega = 0\omega_m$, is caused by associated quantum noises [62]. In the presence of SO-coupling, secondary structure is

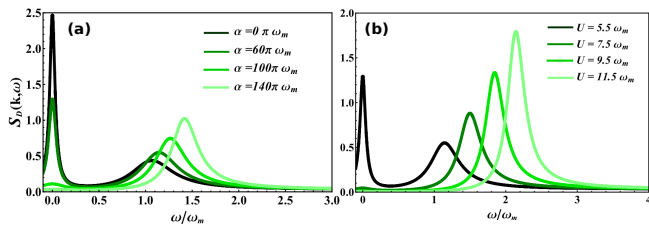


FIG. 6. (Color online) The dynamic structure factor $S_D(k, \omega)$ (in units of $1/Hz$) as a function of ω/ω_m for different strengths of α/ω_m at $U = 5.5\omega_m$ (a) and atom-atom interactions U/ω_m at $\alpha = 10\pi\omega_m$ (b). The input field power ratio is fixed to $P/P_{cr} = 4$ and the remaining coupling strengths are same as in Fig. 5. In (a), the green shaded curves from darkest to lightest correspond to the SO-coupling $\alpha/\omega_m = 0\pi, 60\pi, 100\pi$ and 140π , respectively. Similarly, in (b), green curves (from dark shade to light shade) carry the influence of atom-atom interactions with strengths $U/\omega_m = 5.5, 7.5, 9.5$ and 11.5 , respectively.

shifted to $P \approx 7P_{cr}$ due to the modifications in the inelastic scattering of cavity mode by atomic spin-phase transitions [59], as shown in Fig. 5(b). The spectral densities of both sidebands as well as secondary structure are also increased due to the addition of quasi-particles excited by the SO-coupling.

Dynamic structure factor $S_D(k, \omega)$ at power ratio $P/P_{cr} = 3$ shows two sidebands at $\omega \approx -2\omega_m$ and $\omega \approx 2\omega_m$ corresponding to creation and annihilation of quasi-particles, respectively, as shown in Fig. 5(c). Another, comparatively small, fluctuating structure can be seen at $\omega = 0\omega_m$ induced by the quantum-noise effects which verifies the experimental finding of dynamic structure factor in reference [62]. If we increase the input field power, the dynamic structure factor will be suppressed by the increase in system fluctuations and the sidebands will move towards $\omega = 0\omega_m$, as shown in Fig. 5(d). However, the strength of structure appearing at $\omega = 0\omega_m$ is increased because of quantum noise effects. Interestingly, these effects can be suppressed by SO-coupling because of enhanced intra-cavity atomic back-action, see Fig. 5(e) and 5(f), which leads to the enhancement of sideband spectrum.

In order to further understand influence of SO-coupling as well as cavity mediated long-range atom-atom interactions, we plot $S_D(k, \omega)$ for multiple values of SO-coupling and atom-atom interactions. Fig. 6(a) and 6(b) carry $S_D(k, \omega)$ as a function of normalized frequency for different strengths of α/ω_m and U/ω_m , respectively, at input field power $P/P_{cr} = 5$. It can be clearly seen that by increasing the SO-coupling and atom-atom interactions, the sidebands are enhanced and shifted away from $\omega = 0\omega_m$ due to the addition of quasi-particles. However, quantum noise fluctuations, appearing at $\omega \approx 0$, are now being suppressed by increasing α/ω_m and U/ω_m causing enhancement in optomechanical applications. Here, it should be noted that the strength of atom-atom interactions defines

inter-species as well as intra-species interactions and the frequency of the atomic mode is directly proportional to the strength of interactions \sqrt{U} [23]. Therefore, like SO-coupling, atom-atom interactions have significant influence on the intra-cavity atomic back-action which leads to the enhancement in inelastic scattering of the cavity mode. Thus, the inclusion of SO-coupling purifies dynamic structure factor by squeezing quantum noises.

VII. CONCLUSION

We demonstrate SO-coupling induced back-action cooling in cavity-optomechanics with SO-coupled BEC. The SO-coupling modifies dynamical back-action which enhances low-temperature profile of atomic mode by squeezing associated noises. It has been shown that the existence of SO-coupling leads to cool vibrating end mirror to its quantum mechanical ground state. Further, by computing dynamic structure factor, we have shown that the SO-coupling enables us to manage and implement noiseless quasi-particles. Likewise, mechanical mirror gives rise to the eigenenergy spectrum of atomic states providing control over quantum phase transitions. We chose a particular set of parameters and procedures very close to the present experimental ventures which makes our study experimentally feasible. Our findings constitute a significant step towards the utilization of SO-coupled BEC-optomechanics in the field of quantum optics and quantum information.

ACKNOWLEDGMENT

This work was supported by the NKRDP under grants Nos. 2016YFA0301500, NSFC under grants Nos. 11434015, 61227902, 61378017, KZ201610005011, SKLQOQOD under grants No. KF201403, SPRPCAS under grants No. XDB01020300, XDB21030300. We also acknowledge the financial support from CAS-TWAS president's fellowship programme (2014).

Appendix A: Atomic eigenenergies calculation

Here we provide some details about energy dispersion calculation of atomic states. By adopting a mean-field approximation, we consider the intra-cavity field in steady-state and replace the intra-cavity field operator by its expectation value $\hat{c} \rightarrow \langle c \rangle \equiv c_s$. To calculate energy dispersion E_N of atomic modes, we define E_N as the solution of nonlinear quantum Langevin equations and replace the time derivative id/dt with eigenenergy E_N . After performing some mathematics and applying Pauli matrices, the coupled Langevin equations will take the form [33, 50, 55],

$$n_s = c_s^\dagger c_s = \frac{\eta}{\kappa^2 + (\tilde{\Delta} - \frac{g_m}{\sqrt{2}}(\hat{b}^\dagger + \hat{b}) + g_a(\hat{\varphi}_\uparrow^\dagger \hat{\varphi}_\uparrow + \hat{\varphi}_\downarrow^\dagger \hat{\varphi}_\downarrow))^2}, \quad (\text{A1})$$

$$\hat{b} = \frac{g_m c_s^\dagger c_s}{\sqrt{2}(E_N + i\omega_m + \gamma_m)}, \hat{b}^\dagger = \frac{g_m c_s^\dagger c_s}{\sqrt{2}(E_N - i\omega_m + \gamma_m)}, \quad (\text{A2})$$

$$E_N \begin{pmatrix} \hat{\varphi}_\uparrow \\ \hat{\varphi}_\downarrow \end{pmatrix} = \begin{pmatrix} \frac{\hbar \mathbf{k}^2}{2m} + \frac{\Omega_z}{2} + g_a c_s^\dagger c_s + \frac{1}{2}UN - \gamma_a & -i(\alpha \mathbf{k}_x + \frac{\delta}{2}) + \frac{1}{2}U(\epsilon - 1)\hat{\varphi}_\downarrow^\dagger \hat{\varphi}_\uparrow \\ i(\alpha \mathbf{k}_x + \frac{\delta}{2}) + \frac{1}{2}U(\epsilon - 1)\hat{\varphi}_\uparrow^\dagger \hat{\varphi}_\downarrow & \frac{\hbar \mathbf{k}^2}{2m} - \frac{\Omega_z}{2} + g_a c_s^\dagger c_s + \frac{1}{2}UN - \gamma_a \end{pmatrix} \begin{pmatrix} \hat{\varphi}_\uparrow \\ \hat{\varphi}_\downarrow \end{pmatrix}, \quad (\text{A3})$$

where n_s is the steady-state photon number inside cavity. For simplicity, we have ignored quantum noises associated with the system while calculating eigenenergies of atomic mode. Under number conversation condition $|\hat{\varphi}_\uparrow|^2 + |\hat{\varphi}_\downarrow|^2 = 1$, we substitute steady-state mechanical mirror operators into equ.A1 and simplify in term of n_s as,

$$n_s^3 + 2L_1 L_2 n_s^2 + K n_s = \eta^2 \quad (\text{A4})$$

where,

$$L_1 = \Delta_c + g_a, \quad (\text{A5})$$

$$L_2 = \frac{g_m^2(E_N + \gamma_m)}{(E - n + \gamma_m)^2 + \omega_m^2}, \quad (\text{A6})$$

$$K = \kappa^2 + L_1^2. \quad (\text{A7})$$

Now, by assuming eigenenergies of moving-end mirror and atomic mode independent by keeping mechanical mirror in steady-state, we rewrite equ.A3, for $\hat{\varphi}_\uparrow$ and $\hat{\varphi}_\downarrow$, as,

$$E_N \begin{pmatrix} \hat{\varphi}_\uparrow \\ \hat{\varphi}_\downarrow \end{pmatrix} = \begin{pmatrix} h_1 & w + \frac{1}{2}U(\epsilon - 1)\hat{\varphi}_\downarrow^\dagger \hat{\varphi}_\uparrow \\ w^* + \frac{1}{2}U(\epsilon - 1)\hat{\varphi}_\uparrow^\dagger \hat{\varphi}_\downarrow & h_2 \end{pmatrix} \begin{pmatrix} \hat{\varphi}_\uparrow \\ \hat{\varphi}_\downarrow \end{pmatrix} \quad (\text{A8})$$

where,

$$h_{1,2} = \frac{\hbar \mathbf{k}^2}{2m} \pm \frac{\Omega_z}{2} + g_a n_s + \frac{1}{2}UN - \gamma_a, \quad (\text{A9})$$

$$w = \alpha \mathbf{k}_x + \frac{\delta}{2}. \quad (\text{A10})$$

By dividing first line of equ.A8 with the conjugate of the second line, we obtain,

$$\frac{E_N - h_1}{E_N - h_2} |\hat{\varphi}_\uparrow|^2 = |\hat{\varphi}_\downarrow|^2. \quad (\text{A11})$$

Further, by denoting $s = \frac{E_N - h_1}{E_N - h_2}$ and using number conversation condition, we calculate $|\hat{\varphi}_\uparrow|$ and $|\hat{\varphi}_\downarrow|$ as,

$$|\hat{\varphi}_\uparrow|^2 = \frac{1}{s + 1}, \quad (\text{A12})$$

$$|\hat{\varphi}_\downarrow|^2 = \frac{s}{s + 1}, \quad (\text{A13})$$

and by substituting these values in the first line of equ.A8, we obtain,

$$(E_N - h_1)^2 - \frac{U(\epsilon - 1)(E_N - h_2)s}{s + 1} + \frac{U^2(\epsilon - 1)^2 s^2}{4(s + 1)^2} = s w^2. \quad (\text{A14})$$

Finally, by numerically finding roots of steady-state photon number n_s from equ.A4 and substituting them into equ.A14, we plot the roots of eigenenergies versus quasi-momentum \mathbf{k}_x , as shown in Fig.2. (Note that we consider $\mathbf{k}_y = \mathbf{k}_z = 0$ because SO-coupling is occurring only in the direction of \hat{x} -axis.)

Appendix B: Langevin equations and frequency domain solutions

The coupled Langevin equations of the system contain nonlinear terms in the form of coupling among different degrees of freedom and noises associated with the system. By considering intense external pump field, these equations can be linearized with the help of quantum fluctuations as, $\hat{\mathcal{O}}(t) = \mathcal{O}_s + \delta\mathcal{O}(t)$, where \mathcal{O} can be any operator of the system, \mathcal{O}_s represents steady-state value and $\delta\mathcal{O}(t)$ is the first order quantum fluctuation. During these calculation for simplicity, we assume that both the atomic states, spin- \uparrow and spin- \downarrow , have equal amount of particles, i.e $\hat{\varphi}_\uparrow^\dagger \hat{\varphi}_\uparrow = \hat{\varphi}_\downarrow^\dagger \hat{\varphi}_\downarrow = N/2$. Furthermore, we define system quadratures in the form of dimensionless position and momentum quadratures as, $\hat{q}_O = \frac{1}{\sqrt{2}}(\hat{O} + \hat{O}^\dagger)$ and $\hat{p}_O = \frac{i}{\sqrt{2}}(\hat{O} - \hat{O}^\dagger)$, respectively, (O is generic operator) having commutation relation $[\hat{q}_O, \hat{p}_O] = i$ which reveals the value of scaled Planck's constant $\hbar = 1$. Now the linearized Langevin equation are defined in form of $\dot{\mathcal{X}} = \mathcal{K}\mathcal{X} + \mathcal{F}$, where vector $\mathcal{X} = [\delta q_c(t), \delta p_c(t), \delta q(t), \delta p(t), \delta q_\uparrow(t), \delta p_\uparrow(t), \delta q_\downarrow(t), \delta p_\downarrow(t)]^\tau$ contains position and momentum quadratures of the system (here p and q with \uparrow and \downarrow indicate atomic states, with c indicates cavity mode and without anything indicate mechanical mirror's momentum and position quadrature) and vector $\mathcal{F} = [\sqrt{2\kappa}q_c^{in}, \sqrt{2\kappa}p_c^{in}, 0, 2\sqrt{\gamma_m}f_m, 0, 2\sqrt{\gamma_a}f_a, 0, 2\sqrt{\gamma_a}f_a]^\tau$ defines noises associated with the system. The matrix \mathcal{K} contains dynamical parameters associated with the system,

$$\mathcal{K} = \begin{pmatrix} -\kappa & \Delta & 0 & 0 & 0 & 0 & 0 & 0 \\ \Delta & -\kappa & -G_m & 0 & G_a & 0 & G_a & 0 \\ -2G_m & 0 & -\gamma_m & \omega_m & 0 & 0 & 0 & 0 \\ 0 & 0 & -\omega_m & -\gamma_m & 0 & 0 & 0 & 0 \\ 2G_a & 0 & 0 & 0 & M & \frac{\Omega_z}{2} & (\alpha - \frac{\delta}{2}) & 0 \\ 0 & 0 & 0 & 0 & \frac{\Omega_z}{2} & M & 0 & -(\alpha - \frac{\delta}{2}) \\ 2G_a & 0 & 0 & 0 & (-\alpha + \frac{\delta}{2}) & 0 & M & -\frac{\Omega_z}{2} \\ 0 & 0 & 0 & 0 & 0 & -(-\alpha + \frac{\delta}{2}) & -\frac{\Omega_z}{2} & M \end{pmatrix},$$

where $M = \frac{\Omega}{2} + v + UN(1 - \varepsilon) - \gamma_a$, $v = g_a n_s$ and $\Omega = \hbar \mathbf{k}^2 / m_a$ is the recoil frequency of atomic states. $\alpha = \tilde{\alpha} \mathbf{k}_x$ is the effective strength of SO-coupling. The evolution of the system can be analyzed by matrix \mathcal{K} which contains multiple crucial parameters such as effective detuning $\Delta = \tilde{\Delta} - g_m q_s + g_a N$, where q_s is steady-state quadratures of mechanical mirror, and modified coupling of intra-cavity optical mode with mechanical mirror $G_m = \sqrt{2} g_m |c_s|$ and atomic modes $G_a = \sqrt{2} g_a |c_s|$, tuned by the mean intra-cavity field with amplitude $c_s = \frac{\eta}{\kappa + i\Delta}$. The particular interlaced nature of these steady-state parameters provides an efficient opportunity to understand nonlinear and bistable dynamics of the system.

To make the system accurate and useful, we have to ensure stability of the system and for this purpose, we perform stability analysis of the system. The system can only be stable if the roots of the characteristic polynomial of matrix \mathcal{K} lie in the left half of the complex plane. For this purpose, we apply Routh-Hurwitz Stability Criterion [22] on matrix \mathcal{K} and numerically develop stability conditions for the system. These stability conditions are given as, $M > \kappa + \gamma_m$, $(\alpha - \delta/2)^2 + M^2 > \kappa^2 + \Delta^2 - \omega_m^2 - \Omega_z^2$, $\omega_m > \Delta > \kappa > \gamma_m > 0$ and $\Delta G_a^2 + \Delta G_m^2 > M(\kappa^2 - \Omega_z^2)$. We strictly follow these conditions while performing all numerical calculations in the manuscript.

Furthermore, we take Fourier transform of linearized Langevin equations to preform frequency domain analysis and solve them for position and momentum quadratures of intra-cavity field,

$$\delta q_c(\omega) = \frac{1}{L(\omega)} \left(\sqrt{2\kappa} [\Delta \delta p_c^{in} + (\kappa + i\omega) \delta q_c^{in}] + \Delta [G_a \delta q_{\uparrow}(\omega) + G_a \delta q_{\downarrow}(\omega) - G_m \delta q(\omega)] \right), \quad (\text{B1})$$

$$\delta p_c(\omega) = \frac{1}{L(\omega)} \left(\sqrt{2\kappa} [\Delta \delta q_c^{in} + (\kappa + i\omega) \delta p_c^{in}] + (\kappa + i\omega) [G_a \delta q_{\uparrow}(\omega) + G_a \delta q_{\downarrow}(\omega) - G_m \delta q(\omega)] \right), \quad (\text{B2})$$

respectively, position quadrature of atomic modes,

$$\delta q_{\uparrow, \downarrow}(\omega) = \frac{1}{X(\omega)} \left((B_{\uparrow, \downarrow}(\omega) + A_{\downarrow, \uparrow}(\omega)) C(\omega) [\Delta \delta p_c^{in} + (\kappa + i\omega) \delta q_c^{in}] + L_{1,3}(\omega) f_m + L_{2,4}(\omega) f_a \right), \quad (\text{B3})$$

and finally for the position quadrature of mechanical mirror,

$$\delta q(\omega) = \frac{1}{X_m(\omega)} \left(A_m(\omega) [\Delta \delta p_c^{in} + (\kappa + i\omega) \delta q_c^{in}] + B_m(\omega) f_m + C_m(\omega) f_a \right). \quad (\text{B4})$$

The parameter $L(\omega) = (\kappa + i\omega)^2 - \Delta^2$ contains effective detuning of the system, $W(\omega) = \gamma_a + i\omega - \Omega/2 - v - UN(1 - \varepsilon)$, $K(\omega) = W^2(\omega) + (\alpha^2 - \delta/2)^2$ describes atom-atom interactions and $S_m(\omega) = (\gamma_m + i\omega)^2 L(\omega) - L(\omega) \omega_m^2 + 2G_m^2 \Delta (\gamma_m + i\omega)$ is related to mirror coupling with intra-cavity field. $A_{\uparrow, \downarrow}(\omega) = 4W(\omega)K(\omega)L(\omega)S_m(\omega) \pm \Omega_z^2 L(\omega)S_m(\omega) - 8G_a^2 \Delta K(\omega)S_m(\omega) + 16G_a^2 \Delta^2 G_m^2 (\gamma_m + i\omega)K(\omega)$ and $B_{\uparrow, \downarrow}(\omega) = \pm \Omega_z^2 L(\omega)S_m(\omega) + 4(\pm \alpha \mp \delta/2)K(\omega)L(\omega)S_m(\omega) + 8G_a^2 \Delta K(\omega)S_m(\omega) - 16G_a^2 \Delta^2 G_m^2 (\gamma_m + i\omega)K(\omega)$ describes the behavior of atomic mode and its association with moving-end mirror of the system. $B_m(\omega) = 2G_m \sqrt{(2\kappa)} (\gamma_m + i\omega) X(\omega) + 2G_m \Delta G_a (A_{\uparrow}(\omega) + A_{\downarrow}(\omega) + B_{\uparrow}(\omega) + B_{\downarrow}(\omega))$ represents mechanical mirror behavior and its coupling with atomic modes. Further, $C(\omega) = 8G_a^2 \sqrt{(2\kappa)} K(\omega)S_m(\omega) + 16G_a^2 \sqrt{2\kappa} G_m^2 (\gamma_m + i\omega)K(\omega)$, $L_{1,3}(\omega) = (B_{\uparrow, \downarrow}(\omega) + A_{\downarrow, \uparrow}(\omega)) 8G_a^2 \sqrt{\gamma_m} \Delta K(\omega)L(\omega)(\gamma_m + i\omega)$, $L_{2,4}(\omega) = (B_{\uparrow, \downarrow}(\omega) + A_{\downarrow, \uparrow}(\omega)) 8G_a^2 \sqrt{\gamma_a} K(\omega)S_m(\omega)$, $B_m(\omega) = 2G_m \Delta G_a (L_1(\omega) + L_3(\omega)) + 2\sqrt{\gamma_m} L(\omega)X(\omega)$ and $C_m(\omega) = 2G_m \Delta G_a (L_2(\omega) + L_4(\omega))$. The term $X(\omega) = A_{\uparrow}(\omega)A_{\downarrow}(\omega) + B_{\uparrow}(\omega)B_{\downarrow}(\omega)$ represents modified susceptibility atomic states and $X_m(\omega) = X(\omega)S_m(\omega)$ corresponds to the modified susceptibility of mechanical mirror.

Appendix C: Density-noise spectrum (DNS)

By using frequency domain solutions given above and standard formalism for auto-correlation, $S_{\mathcal{O}} = \frac{1}{2\pi} \int e^{-i(\omega - \dot{\omega})} \langle \mathcal{O}(\omega) \mathcal{O}(\dot{\omega}) \rangle d\dot{\omega}$, as discussed in main text, where $\mathcal{O}(\omega)$ is the generic operator, the DNS for pseudo

spin- \uparrow and spin- \downarrow atomic states will be read as,

$$S_{\uparrow,\downarrow}(\omega, \Delta) = \frac{1}{|X(\omega)|^2} \left(2\pi|C(\omega)|^2(|B_{\uparrow,\downarrow}(\omega)|^2 + |A_{\downarrow,\uparrow}(\omega)|^2)[\Delta^2 + \kappa^2 + \omega^2] + 2\pi L_{2,4}(\omega) + L_{1,3}(\omega) \frac{\gamma_m \omega}{\omega_m} [1 + \text{Coth}(\frac{\hbar\omega}{2k_B T})] \right). \quad (\text{C1})$$

Similarly, we can write DNS equation for mechanical mirror of the system as,

$$S_m(\omega, \Delta) = \frac{1}{|X_m(\omega)|^2} \left(|A_m(\omega)|^2(\Delta^2 + \kappa^2 + \omega^2) + 2\pi B_m(\omega) + C_m(\omega) \frac{\gamma_m \omega}{\omega_m} [1 + \text{Coth}(\frac{\hbar\omega}{2k_B T})] \right). \quad (\text{C2})$$

Appendix D: Spectral density of out-going optical field

In order to calculate output optical field of the system, we use input-output field relation, $\delta q_c^{out} = \sqrt{2\kappa} \delta q_c - \delta q_c^{in}$ and $\delta p_c^{out} = \sqrt{2\kappa} \delta p_c - \delta p_c^{in}$, where p_{in}, q_{in} and p_{out}, q_{out} represent input and output field quadratures, respectively. By utilizing above relation and intra-cavity field quadrature, we obtain output field relation as,

$$\delta q_c^{out}(\omega) = \frac{1}{L(\omega)} \left([2\kappa\Delta\delta p_c^{in} + (\kappa^2 + \omega^2 + \Delta^2)\delta q_c^{in}] + \sqrt{2\kappa}\Delta[G_a\delta q_{\uparrow}(\omega) + G_a\delta q_{\downarrow}(\omega) - G_m\delta q(\omega)] \right), \quad (\text{D1})$$

$$\delta p_c^{out}(\omega) = \frac{1}{L(\omega)} \left([2\kappa\Delta\delta q_c^{in} + (\kappa^2 + \omega^2 + \Delta^2)\delta p_c^{in}] + \sqrt{2\kappa}(\kappa + i\omega)[G_a\delta q_{\uparrow}(\omega) + G_a\delta q_{\downarrow}(\omega) - G_m\delta q(\omega)] \right). \quad (\text{D2})$$

Now, by combining position and momentum quadratures of field, we obtain out-going field operator c_{out} as,

$$\delta c_{out}(\omega) = \frac{1}{L(\omega)} \left([2\kappa\Delta\delta c_{in}^{\dagger} + (\kappa^2 + \omega^2 + \Delta^2)\delta c_{in}] + \sqrt{2\kappa}\Delta[G_a\delta q_{\uparrow}(\omega) + G_a\delta q_{\downarrow}(\omega) - G_m\delta q(\omega)] \right). \quad (\text{D3})$$

Further, to determine the dependence of out-going optical mode on the external pump field power P , we redefine

coupling terms as a function of P ,

$$G_m = \sqrt{2}C_S g_m = \frac{2\omega_c}{L} \sqrt{\frac{P\kappa}{m\omega_m\omega_p(\kappa^2 + \Delta^2)^2}}, \quad (\text{D4})$$

$$G_a = \sqrt{2}C_S g_a = \frac{2\omega_c}{L} \sqrt{\frac{P\kappa}{m\Omega\omega_p(\kappa^2 + \Delta^2)^2}}, \quad (\text{D5})$$

and after this, we calculate Density-noise spectrum (DNS) of out-going optical mode by simply using two frequency auto-correlation formula,

$$S_{out}(P, \omega) = \frac{2\pi}{|L(\omega)|^2} \left([\kappa^2 + \omega^2 + \Delta^2 + 2\kappa\Delta] + 4\kappa\Delta[G_a S_{\uparrow}(\omega, \Delta) + G_a S_{\downarrow}(\omega, \Delta) - G_m \delta S_m(\omega, \Delta)] \right). \quad (\text{D6})$$

Appendix E: Influence of atom-atom interactions on atomic density-noise spectrum

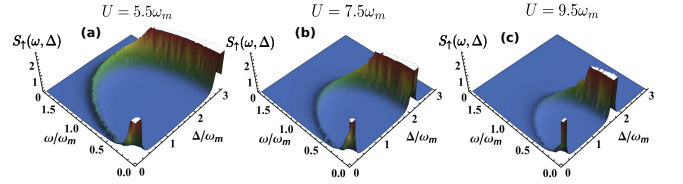


FIG. 7. (Color online) The dynamics of $S_{\uparrow}(\omega, \Delta)$, as a function of detuning Δ/ω_m and frequency ω/ω_m , under the effects of many-body interactions U/ω_m . (a), (b) and (c) demonstrate $S_{\uparrow}(\omega, \Delta)$ with atom-atom interaction $U = 5.5\omega_m, 7.5\omega_m$ and $9.5\omega_m$, respectively. Here, the strength of SO-coupling is kept constant $\alpha = 10\pi\omega_m$. One can observe that the strength of atom-atom interactions influences $S_{\uparrow}(\omega, \Delta)$ in a similar way as SO-coupling does. By increasing U/ω_m , the area underneath $S_{\uparrow}(\omega, \Delta)$ is decreased which leads to the cooling of atomic mode [23]. The remaining parameters are same as in Fig. 2.

The atom-atom interactions U/ω_m of atomic dressed states show similar influence on $S_{\uparrow}(\omega, \Delta)$ as the influence of SO-coupling on the atomic dressed states, which can be seen in Fig. 7(a-c), where the strength of atom-atom interactions is considered as, $U = 5.5\omega_m, 7.5\omega_m, 9.5\omega_m$, respectively. The radius as well as height of the atomic DNS decreases with increase in atom-atom interactions U/ω_m of dressed states. (Note: The effects of atom-atom interactions $S_{\downarrow}(\omega, \Delta)$ are not shown here because they will be like-wise as on $S_{\uparrow}(\omega, \Delta)$.) As atom-atom interactions are the combination of inter-species as well as intra-species interactions and modifies the coupling atomic states with intra-cavity potential, therefore, by increasing interactions, the strength of atomic back-action will be increased leading to more self confinement. Thus, the strength of atom-atom interactions can likely be used to

control the low-temperature dynamics of atomic dressed states as SO-coupling.

Appendix F: Mirror density-noise spectrum under influence of SO-coupling and atom-atom interactions

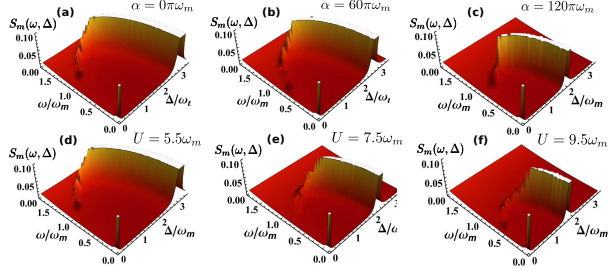


FIG. 8. (Color online) Density-noise spectrum (DNS) $S_m(\omega, \Delta)$ (in units of W/Hz) for mechanical mirror of the system versus normalized effective detuning Δ/ω_m and frequency ω/ω_m under the influence of spin-orbit (SO) coupling α/ω_m of atomic spin-states and normalized atom-atom interactions U/ω_m among atomic states. (a) Demonstrates $S_m(\omega, \Delta)$ in the absence of SO-coupling $\alpha = 0\pi\omega_m$ with atom-atom interactions $U = 5.5\omega_m$. The color configuration corresponds to the strength of mechanical mirror DNS ($S_m(\omega, \Delta)$). (b) and (c) illustrate the behavior of $S_m(\omega, \Delta)$ under the influence of $\alpha = 60\pi\omega_m$ and $120\pi\omega_m$, respectively. The dynamics of $S_m(\omega, \Delta)$ under the effects of many-body interactions U/ω_m are illustrated in (d-f). (d), (e) and (f) demonstrate $S_m(\omega, \Delta)$ as a function of Δ/ω_m and ω/ω_m with atom-atom interaction $U = 5.5\omega_m, 7.5\omega_m$ and $9.5\omega_m$, respectively, while the strength of SO-coupling is kept constant $\alpha = 10\pi\omega_m$. The atom-field coupling is considered as $G_a = 4.1\omega_m$ while the mirror-field coupling is taken as $G_m = 1.5\omega_m$. The remaining parameters, used in numerical calculations, are same as in Fig. 2.

The dynamics of mechanical mirror will also be influenced by the existence of atomic-states as atomic dressed states are influenced by the existence of mechanical mirror. Fig. 8 demonstrates $S_m(\omega, \Delta)$ as a function of Δ/ω_m and ω/ω_m , under the influence of SO-coupling and atom-atom interaction. The atom-field coupling is considered as $G_a = 4.1\omega_m$ while the mirror-field coupling is taken as $G_m = 1.5\omega_m$. The behavior of $S_m(\omega, \Delta)$ in the absence of SO-coupling is shown in Fig. 8(a), which is similar to the behavior of atomic DNS. A semi-circular structure appears with increase in detuning Δ/ω_m towards frequency ω/ω_m . The height of $S_m(\omega, \Delta)$ decreases initially and achieves optimal cooling point. However, when the system detuning is further increased from $\Delta = 1\omega_m$, the $S_m(\omega, \Delta)$ shows rapid increase in the height of structure giving rise to the temperature of mechanical mirror.

The strength of SO-coupling induces similar influence as it does on the atomic DNS. The radius of the structure is suppressed by the increased SO-coupling, as shown in Fig. 8(b) and 8(c), where the strength of SO-coupling is increased to $\alpha = 60\omega_m$ and $130\omega_m$, respectively. Not

only SO-coupling but also the atom-atom interactions of atomic dressed states will show similar effects on mechanical DNS as they are inducing in atomic DNS. The increase in atom-atom interactions will also reduce the radius of semi-circular structure, as shown in Fig. 8(d), 8(e) and 8(f), where the strength of atom-atom interactions is increased to $U = 5.5\omega_m, 7.7\omega_m$ and $9.5\omega_m$, respectively. The SO-coupling and atom-atom interactions modify the atomic density mode excitation leading to the variation in intra-cavity optical spectrum in the form of modified atomic back-action which will consequently lead to the absorption of more mirror excitations by spin states. It can also be considered as the atomic and mechanical states are connected with each other through intra-cavity radiation pressure, acting as a spring between these two independent entities, therefore, the modifications produced by SO-coupling and atom-atom interaction will show similar influence on mechanical mirror as they are producing on atomic dressed states [23].

Appendix G: Influence of atom-field coupling and atom-atom interactions on mechanical mirror temperature

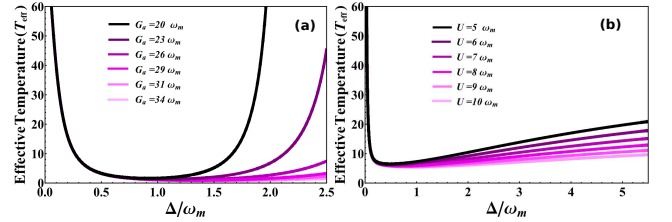


FIG. 9. (Color online) (a) Illustrates the effective-temperature T_{eff} of mechanical mirror under the influence of G_a/ω_m . The SO-coupling strength is now considered as $\alpha = 100\pi\omega_m$ and many-body interaction is kept as $U = 5.5\omega_m$. The black curve represents $G_a = 20\omega_m$ while magenta curves from dark shade to light shade are for atom-field coupling $G_a = 23\omega_m, 26\omega_m, 29\omega_m, 31\omega_m$ and $34\omega_m$, respectively. Similarly, (c) deals with the behavior effective-temperature T_{eff} of mechanical mirror under the influence of U/ω_m at $\alpha = 100\pi\omega_m$ and $G_a = 20\omega_m$. Similarly, the black curve represents $U = 5\omega_m$ while magenta curves from dark shade to light shade represent atom-atom interactions $U = 6\omega_m, 7\omega_m, 8\omega_m, 9\omega_m$ and $10\omega_m$, respectively. The other parameters used in numerical calculation are same as in Fig. 2.

If we increase the atomic mode coupling with intra-cavity field, atomic dressed states will absorb more phonons emitted by mechanical mirror of the system which will decrease the thermal excitation of mechanical mirror. Fig. 9(a) shows such influence of atom-field coupling on mechanical oscillator of the system where the effective-temperature of mirror is decreased by increasing atom-field coupling [21]. The atom-atom interactions of atomic mode will also influence the mechanical mirror

similarly as SO-coupling has shown [23]. The atom-atom interactions also contribute to control the thermal exci-

tation of mechanical mirror which lead to cool oscillating mirror to its quantum mechanical ground state, as shown in Fig.9(b).

-
- [1] T. J. Kippenberg, and K. J. Vahala, *Science* **321**, 1172 (2008); M. Aspelmeyer, T. J. Kippenberg, and F. Marquardt, *Rev. Mod. Phys.* **86**, 1391 (2014).
 - [2] T. J. Kippenberg, and K. J. Vahala, *Optics Express* **17**, 20911 (2009).
 - [3] P. Meystre, *Annalen der Physik* **525**, 215 (2013).
 - [4] A. D. O'Connell *et al.*, *Nature* **464**, 697 (2010).
 - [5] J. D. Teufel *et al.*, *Nature* **475**, 359 (2011).
 - [6] J. Chan *et al.*, *Nature* **478**, 89 (2011).
 - [7] M. Yuan *et al.*, *Nat. Commun.* **6**, 8491 (2015).
 - [8] O. Arcizet *et al.*, *Nature* **444**, 71 (2006).
 - [9] S. Gigan *et al.*, *Nature* **444**, 67 (2006).
 - [10] D. Kleckner, and D. Bouwmeester, *Nature* **444**, 75 (2006).
 - [11] A. Schliesser *et al.*, *Phys. Rev. Lett.* **97**, 243905 (2006).
 - [12] J. D. Teufel *et al.*, *Phys. Rev. Lett.* **101**, 197203 (2008).
 - [13] D. J. Wilson *et al.*, *Nature* **524**, 325 (2015).
 - [14] I. Wilson-Rae *et al.*, *Phys. Rev. Lett.* **99**, 093901 (2007).
 - [15] E. E. Wollman *et al.*, *Science* **349**, 852-855 (2015).
 - [16] A. Nigués, A. Siria, and P. Verlot, *Nat. Commun.* **6**, 8104 (2015).
 - [17] K. W. Murch *et al.*, *Nature Physics* **4**, 561 (2008).
 - [18] F. Brennecke *et al.*, *Science* **322**, 235 (2008).
 - [19] K. A. Yasir, and W. M. Liu, *Sci. Rep.* **5**, 10612 (2015).
 - [20] K. A. Yasir, and W. M. Liu, *Sci. Rep.* **6**, 22651 (2016).
 - [21] M. Paternostro *et al.*, *New J. Phys.* **8**, 107 (2006).
 - [22] M. Paternostro, G. D. Chiara, and G. M. Palma, *Phys. Rev. Lett.* **104**, 243602 (2010).
 - [23] S. Mahajan, N. Aggarwal, A. B. Bhattacharjee, and Man-Mohan, *J. Phys. B: At. Mol. Opt. Phys.* **46**, 085301 (2013).
 - [24] Y. C. Liu *et al.*, *Phys. Rev. Lett.* **110**, 153606 (2013).
 - [25] Florian Elste, S. M. Girwin, and A. A. Clerk, *Phys. Rev. Lett.* **102**, 207209 (2009).
 - [26] D. W. C. Brooks *et al.*, *Nature* **488**, 476 (2012).
 - [27] K. Zhang, F. Bariani, and P. Meystre, *Phys. Rev. Lett.* **112**, 150602 (2014).
 - [28] A. H. Safavi-Naeini *et al.*, *New J. Phys.* **15**, 035007 (2013).
 - [29] Y. Yanay, J. C. Sankey, and A. A. Clerk, *Phys. Rev. A* **93**, 063809 (2016).
 - [30] P. Weber *et al.*, *Nat. Commun.* **7**, 12496 (2016).
 - [31] V. Galitski, and I. B. Spielman, *Nature* **494**, 49 (2013).
 - [32] X.J. Liu *et al.*, *Phys. Rev. Lett.* **102**, 046402 (2009).
 - [33] Y. J. Lin *et al.*, *Nature* **462**, 628 (2009).
 - [34] Y. K. Kato *et al.*, *Science* **306**, 1910-1913 (2004).
 - [35] M. König *et al.*, *Science* **318**, 766-770 (2007).
 - [36] B. A. Bernevig, T. L. Hughes, and S. C. Zhang, *Science* **314**, 1757-1761 (2006).
 - [37] D. Hsieh, *et al.*, *Nature* **452**, 970-974 (2008).
 - [38] X. Li, E. Zhao, and W. V. Liu, *Nat. Commun.* **4**, 4023 (2013).
 - [39] K. Sun *et al.*, *Nat. Phys.* **8**, 67-70 (2012).
 - [40] J. D. Koralek *et al.*, *Nature* **458**, 610-613 (2009).
 - [41] C. Hamner, *Phys. Rev. Lett.* **114**, 070401 (2015).
 - [42] Y. J. Lin, K. Jiménez-García, and I. B. Spielman, *Nature* **471**, 83 (2011).
 - [43] H. Hu *et al.*, *Phys. Rev. Lett.* **108**, 010402 (2012).
 - [44] L. Jiang *et al.*, *Phys. Rev. A* **90**, 053606 (2014).
 - [45] X. F. Zhou *et al.*, *Phys. Rev. A* **91**, 033603 (2015).
 - [46] Z. Cai, X. Zhou, and C. Wu, *Phys. Rev. A* **85**, 061605(R) (2012).
 - [47] S. W. Su *et al.*, *Phys. Rev. A* **86**, 023601 (2012); S. W. Su *et al.*, *ibid.* **84**, 023601 (2011).
 - [48] Y. Y. Xiang, J. Ye, and W. M. Liu, *Phys. Rev. A* **90**, 053603 (2014); S. S. Zhang *et al.*, *ibid.* **87**, 063623 (2013).
 - [49] N. Goldman *et al.*, *Rep. Prog. Phys.* **77**, 126401 (2014).
 - [50] J. Dalibard *et al.*, *Rev. Mod. Phys.* **83**, 1523 (2011).
 - [51] X. Zhou, Y. Li, Z. Cai, and C. Wu, *J. Phys. B: At. Mol. Opt. Phys.* **48**, 249501 (2015).
 - [52] C. Wu, M. S. Ian, X. F. Zhou, *Chin. Phys. Lett.* **28**, 097102 (2011).
 - [53] Y. Deng *et al.*, *Phys. Rev. Lett.* **112**, 143007 (2014).
 - [54] B. Padhi, and S. Ghosh, *Phys. Rev. A* **90**, 023627 (2014).
 - [55] L. Dong *et al.*, *Phys. Rev. A* **89**, 011602(R) (2014).
 - [56] L. Dong, C. Zhu, and H. Pu, *Atoms* **3**(2), 182-194 (2015).
 - [57] J. S. Bennett *et al.*, *New J. Phys.* **18**, 053030 (2016).
 - [58] I. Wilson-Rae *et al.*, *New J. Phys.* **10**, 095007 (2008).
 - [59] M. Punk, D. Chowdhury, and S. Sachdev, *Nat. Phys.* **10**, 289 (2014).
 - [60] H. Miyake *et al.*, *Phys. Rev. Lett.* **107**, 175302 (2011).
 - [61] S. Sachdev, *Science* **288**, 475-480 (2000).
 - [62] R. Landig *et al.*, *Nat. Commun.* **6**, 7046 (2015).
 - [63] A. L. Fetter, *Phys. Rev. A* **89**, 023629 (2014).
 - [64] C. Maschler, I. B. Mekhov, and H. Ritsch, *Eur. Phys. J. D* **46**, 545-560 (2008).
 - [65] J. Higbie, and D. M. Stamper-Kurn, *Phys. Rev. A* **69**, 053605 (2004).
 - [66] S. Fölling *et al.*, *Nature* **434**, 481-484 (2005).
 - [67] J. M. Pirkkalainen *et al.*, *Nat. Commun.* **6**, 6981 (2015).
 - [68] G. Birkel *et al.*, *Phys. Rev. Lett.* **75**, 2823 (1995).
 - [69] H. Miyake *et al.*, *Phys. Rev. Lett.* **107**, 175302 (2011).